water

MDPI

Article

Modeling Study on the Hydrodynamic Environmental Impact Caused by the Sea for Regional Construction near the Yanwo Island in Zhoushan, China

He Gou [1,2], Feng Luo [1,3,*], Ruijie Li [1,2,*], Xiaotian Dong [4] and Yifeng Zhang [5]

1 Key Laboratory of Coastal Disaster and Defence, Ministry of Education, Hohai University, Nanjing 210098, China
2 College of Oceanography, Hohai University, Nanjing 210098, China
3 College of Harbour, Coastal and Offshore Engineering, Hohai University, Nanjing 210098, China
4 School of Civil and Ocean Engineering, Huaihai Institute of Technology, Lianyungang 222005, China
5 Tianjin Research Institute for Water Transport Engineering, Tianjin 300000, China
* Correspondence: fluo@hhu.edu.cn (F.L.); rjli2001@163.com (R.L.)

Received: 1 July 2019; Accepted: 9 August 2019; Published: 13 August 2019

check for updates

Abstract: Waves are one of the most important factors affecting offshore marine engineering. Accurate calculation of wave distribution is an important prerequisite to ensure the safety of coastal engineering construction. Due to the influence of complex topography, hydrological conditions, and marine structures on the propagation of waves offshore, slowly varying topography, refraction, diffraction, reflection, shallowness, and other phenomena may occur. This article combines the *MIKE21 Spetral Waves* (SW) wave model and the *MIKE21 Boussinesq Waves* (BW) wave model which are developed by Danish Hydraulic Institute (DHI) for a joint application (SW–BW nested model). It simulates the hydrodynamic environment of the Yanwo Island scenic area, located in Zhoushan, in both large and small ranges. In addition, wave height distribution and berthing stability of different breakwater planning schemes are calculated to optimize the layout of the breakwater. Through the analysis of simulation results, it is concluded that the hydraulic performance of Scheme 2 (the broken line section on the west side is 100 m long, and that on the east is 1200 m long, and the breakwater is rotated 8 degrees counterclockwise along the axis on the basis of Scheme 1) is better than that of Scheme 1 (the broken line section on the west side is 100 m long, and that on the east is 1100 m long), which can provide a more reliable construction reference for the construction of the Yanwo Island scenic area.

Keywords: SW–BW nested model; optimization of breakwater layout; wave height distribution; berthing stability; numerical simulation

1. Introduction

It is of great theoretical significance and application value to study the motion law of waves, especially for shipping, port, and ocean engineering. At present, the main mathematical models for studying waves are plane two-dimensional wave models, vertical two-dimensional wave models, and three-dimensional wave models [1,2]. The plane two-dimensional wave theory is the most widely applied theory in the current wave research, and software such as MIKE, Hindcast Shallow Water Waves (HISWA), Simulation Waves Nearshore (SWAN), and Conjugate Gradient Waves (CGWAVE) have appeared to support it [3]. According to different control equations, the plane two-dimensional wave theory can be divided into the energy balance equation model, mild-slope equation model, Boussinesq equation model, and Navier–Stokes equation model [4–6]. The energy balance equation model, which is based on the principle of conservation of energy, is currently in the third generation [7–9]. It can depict the generation, growth, and attenuation of wind waves by calculating spatial distribution of spectrum. It is only applicable to the region with a large scale because the calculation accuracy in local, complex topographic waters is low. The Boussinesq equation, which is obtained by simplified treatment according to the Navier–Stokes equation, can directly describe the movement of water particles [10]. It can calculate the motion of water particles with the advantage of higher accuracy but disadvantages of heavy calculation burden and complex boundary conditions.

Field observation, physical model test, and numerical simulation are the main methods to study wave propagation. Compared with the physical model test and field observation, the numerical simulation method has developed rapidly due to its advantages such as low cost, flexible application, short period, freedom from the influence of scale effect, and availability in a test environment [11].

Chinese and foreign scholars have made improvements in wave nonlinearity, diffraction, bottom friction, wave energy loss, irregularity, and calculation methods [12–15]. The improved models have been widely used worldwide and in local areas to analyze the characteristics and propagation laws of wave fields [16–28]. Wang et al. [29] combined the SWAN model based on the energy balance equation with the CGWAVE model based on the mild-slope equation, which has a good adaptability in wave calculation of Dong Fushan Island. Wang et al. [30] used the modified Boussinesq equation of *MIKE21* Boussinesq *Waves (BW)* to calculate wave height distribution behind the breakwater in the Xiaoguoju fishing port project, and optimized eight layouts of breakwaters to select the best one. Xu et al. [31] used the Boussinesq equation to compare and analyze the influence of different channel conditions and wave incident directions on wave fields on a small scale, and obtained the regularities of wave distributions in the harbor. Ji and Dong [32] used a wave model based on the energy balance equation to study wave transmission and overtopping around nearshore breakwaters. Sea level data series obtained from the nodes of the mesh of a hydrodynamic model (virtual tide gauges) were used to study the estuarine environment for port construction and navigation [33]. Broken wave characteristics in front of a vertical seawall were modeled and studied by using a Total Variation Diminishing Version of the Fully Nonlinear Boussinesq Wave Model (FUNWAVE-TVD) [34].

The spatial and temporal distribution of wave height is affected by the implementation of sea planning for regional construction, and it may cause severe damage to offshore engineering. Accordingly, research on the change of wave height before and after the oceanographic engineering can not only effectively reduce potential hazards, but also improve the rationality of the layout planning of marine engineering to increase economic benefits.

In this paper, the energy balance equation and the Boussinesq equation are combined to calculate wave parameters around the nearshore of a proposed breakwater and pier, and a better plane layout of the breakwater is selected according to the simulation results. This study can provide reliable results for the designing institute to reduce potential disasters.

2. Research Background

The study area is located in the northeast of Zhoushan City, Zhejiang Province of China between 30°07′ N and 30°38′ N and 121°31′ E and 123°17′ E. Daishan County covers a sea area of 4916 square kilometers, which accounts for about 93.7% of the total area of the county. Daishan county is composed of 404 islands with different sizes, and all islands show the southwest-northeast trend (“X” type distribution) centered on Daishan Island, about 169.6 km long from east to west and 57 km wide from north to south (Figure 1). The topography of the target sea area is shown in Figure 2. In order to make full use of island resources to promote the development of natural scenic-spot tourism and increase the economic benefits of Zhoushan, construction of a land–island transportation terminal project in Yanwo scenic area at the north end of Daishan Island has been proposed, including a pier and a breakwater. The terminal will effectively ensure water transfer and satisfy the demand of waterway passenger transport in the north part of Zhoushan.

In order to provide a scientific basis of engineering design and implementation for relevant departments, it is necessary to calculate wave parameters on both sides of the proposed breakwater.

In addition, berthing stability conditions must also be judged to further optimize the layout of the breakwater, which can improve the rationality of the layout of sea planning for regional construction.

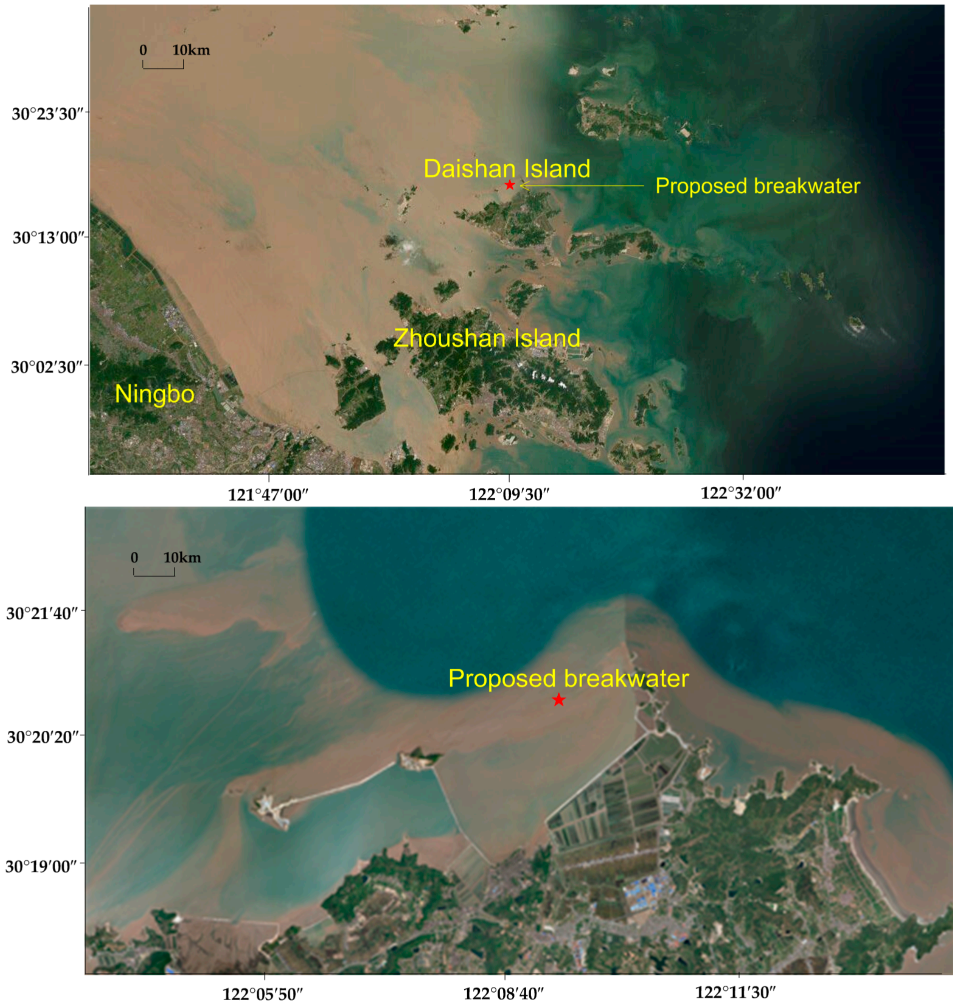

Figure 1. Geographic environment in survey region.

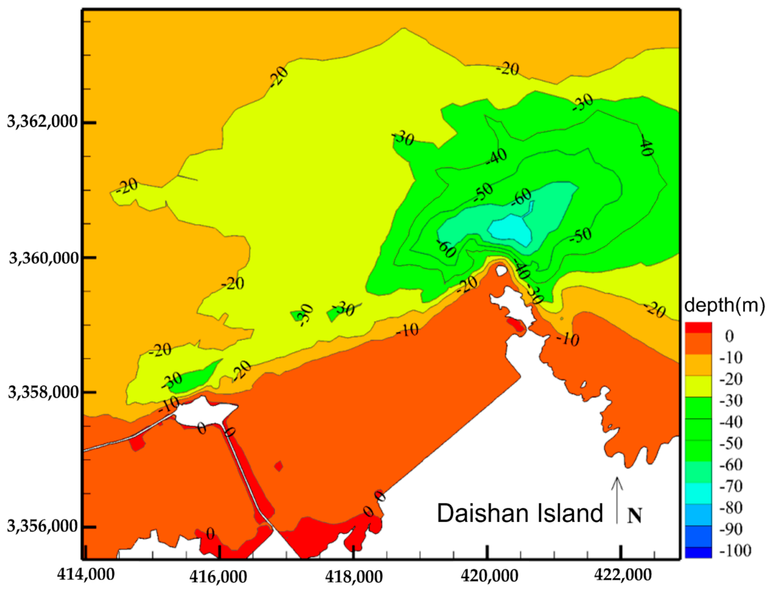

Figure 2. Underwater topographic map of the engineering area.

2.1. Meteorological Conditions in the Engineering Area

Daishan Island stands in the monsoon ocean climate zone of the north subtropical. There are various kinds of landforms such as sandy beaches, shoals, and hills on the island with moist air, sufficient light, suitable temperature, but less precipitation. The annual average wind speed is 6.6 m/s, the maximum wind speed is 38.6 m/s, the annual average maximum wind speed is 23.37 m/s, and the dominant wind directions are north, northeast, and southeast wind.

Typhoon is the main severe weather system affecting the engineering area due to the alternating warm and cold air. According to the typhoon data from recent decades, the number of typhoons that have an influence on the engineering area varies between 3.5 and 7 per year, on average. The measured maximum wind speed varies between 13.9 m/s and 36.9 m/s, that is to say, the wind scale is between moderate gale and hurricane. Typhoons mainly occur from July to September, accounting for 78% of the total number of typhoons in the whole year.

2.2. Research Methods

Wave distribution in the northern Zhejiang sea area was calculated by adopting a mathematical model that is suitable for simulating wave conditions on a large scale. The incident open boundary conditions that are applicable for calculation on a small scale were extracted when the simulation results were in accordance with the observed data of the wave observation station and weather observation station. Subsequently, the influence of regional construction on the hydrodynamic environment around the coastal islands in Zhoushan was analyzed.

Given the position of the proposed marine structures, hydrodynamic-environment changes near the pier and breakwater before and after the implementation were forecasted under the combination of two kinds of water levels (extreme high water level of 3.3 m, design high water level of 2.3 m), six kinds of wave directions (N, NNE, NE, W, WNW, NW) that are unfavorable to the engineering area, and two return periods (once in 50 years, once in 2 years). By computing wave field distribution, wave parameter changes of the feature points, effective shield area of the breakwater, and berthing state, a better plane-layout plan of the breakwater was selected to promote tourism development of the Yanwo scenic area on Daishan Island.

It should be noted that in order to intuitively reflect the plane span of the breakwater project, the plane-coordinate system was uniformly adopted in meters.

3. Source of the Data Used

3.1. Wind Data

Wind speed data was provided by Jinjimen weather station, which is situated on the Yangshan Island of Zhejiang (Figure 3). Its geographical coordinates are 122°2′ E, 37°30′ N, and it has good representativeness of winds coming from NNW to WSW. The wind speeds of different return periods, which were converted to 10 m above sea level, are shown in Table 1.

Combined with wind speed, the wind–wave growth formula, which is recommended in Technical Regulations on Seawall Engineering of Zhejiang Province [35], are used to infer wave height and period values of NNW to WSW that propagate seaward, and theoretical calculations are used for calibration data of waves on a large scale (Table 2). The wind–wave growth formula is as follows:

$$\frac{g\overline{H}}{V^2} = 0.13th\left[0.7\left(\frac{gd}{V^2}\right)^{0.7}\right]th\left[\frac{0.0018\left(\frac{gF}{V^2}\right)^{0.45}}{0.7\left(\frac{gd}{V^2}\right)^{0.7}}\right], \tag{1}$$

$$\frac{g\overline{T}}{V^2} = 13.9\left(\frac{g\overline{H}}{V^2}\right)^{0.5} \tag{2}$$

where g is the acceleration of gravity; F is fetch length; V is wind speed; d is water depth; $\overline{H}$ is mean wave height; and $\overline{T}$ is mean wave period.

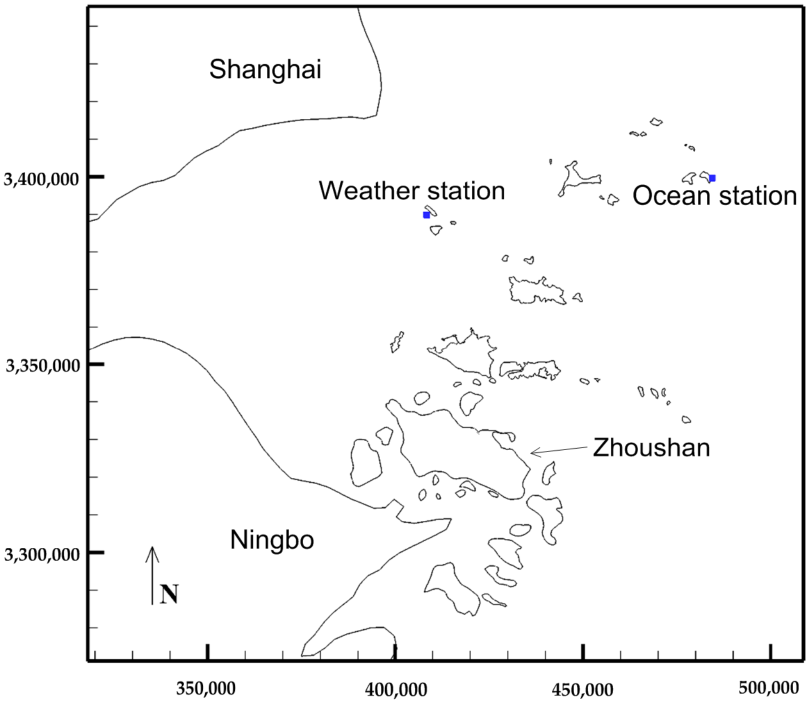

Figure 3. Position of observation stations.

Table 1. Wind speeds at the Jinjimen weather station in different return periods (unit: m/s).

Wind Direction	Once in 50 Years	Once in 2 Years
WSW	28.3	13.9
W	27.4	13.2
WNW	29.7	20.4
NW	26.2	20.1
NNW	35.7	23.5

Table 2. Calibration values of wave parameters in different return periods.

Wave Direction	Hs (m) [1]		Ts (s) [2]	
	Once in 50 Years	Once in 2 Years	Once in 50 Years	Once in 2 years
WSW	3.63	2.04	7.69	5.76
W	3.59	1.99	7.65	5.70
WNW	3.86	2.93	7.93	6.91
NW	3.69	2.98	7.75	6.97
NNW	4.23	3.09	8.30	7.09

Notes: [1] Hs: Significant wave height; [2] Ts: Significant wave period.

3.2. Wave Data

The measured wave data was from Shengshan ocean station (Figure 3). The station lies in the northeast part of Yanwo Island with coordinates of 122°49′ E, 30°42′ N. The maximum wave height and frequency data of 16 directions from 1995 to 2012 provided by the station are only representative of waves coming from N to ESE instead of NNW to WSW.

To make full use of the raw data provided by Jinjimen station, wave height data from N to ESE were used as calibration values for numerical simulation results on a large scale. The measured wave data only contains maximum wave height for a year, but lacks corresponding period values. Since the engineering area is mainly superposed of wind wave and swell, the Formula of Putian Seawall Test Station that is recommended in Technical Regulations on Seawall Engineering of Zhejiang Province was adopted. It was used to calculate the wave height in each return period and its corresponding period value for six directions (Table 3).

Table 3. Calibration values of wave parameters during different return periods.

Wave Direction	Hs (m)		Ts (s)	
	Once in 50 Years	Once in 2 Years	Once in 50 Years	Once in 2 Years
N	4.55	2.92	8.58	6.88
NNE	8.01	2.95	11.38	6.90
NE	10.76	2.90	13.20	6.85
ENE	4.98	3.00	8.98	6.97
E	8.74	2.99	11.82	6.82
ESE	9.93	2.69	12.67	6.59

4. Mathematical Wave Models

4.1. Energy Balance Equation

4.1.1. Governing Equation

The governing equation of the mathematical wave model of the energy balance equation is as follows:

$$\frac{\partial N}{\partial t} + \frac{\partial C_x N}{\partial x} + \frac{\partial C_y N}{\partial y} + \frac{\partial}{\partial \sigma} C_\sigma N + \frac{\partial}{\partial \theta} C_\theta N = \frac{S}{\sigma}, \tag{3}$$

where $N = E/\sigma$, N is the dynamic spectral density, E is the energy spectral density; σ, θ are relative frequency and wave direction, respectively; C_x, C_y, C_σ, C_θ are group velocity on space x, y, σ, θ, respectively; t is time; $S = S_{in} + S_{nl} + S_{ds} + S_{bot} + S_{surf}$; and S_{in}, S_{nl}, S_{ds}, S_{bot}, and S_{surf} represent the wind energy input term, nonlinear wave interaction term, white wave dissipation term, bottom friction term, and wave breaking dissipation term, respectively.

4.1.2. Selection of Calculation Parameters

The incident wave uses the Joint North Sea Wave Project (JONSWAP) spectrum to simulate irregular waves, which is defined as

$$S(f) = \alpha H_S{}^2 T_P{}^{-4} f^{-5} \exp(-\frac{5}{4}(T_P f)^{-4}) \times \gamma^{\exp(-(f/f_p - 1)^2/2\sigma^2)}, \tag{4}$$

among them

$$\alpha = \frac{0.06238}{0.230 + 0.0336\gamma - 0.185(1.9+\gamma)^{-1}}(1.094 - 0.01915 \ln \gamma) \text{ and} \tag{5}$$

$$T_P = \overline{T}/(1 - 0.532(\gamma + 2.5)^{-0.569}), \tag{6}$$

where T_P is the peak period; H_S is the significant wave height; $\overline{T}$ is the average period; γ is the spectral peak raising factor, and the value in standard JONSWAP spectrum is 3.3.

The bottom friction coefficient is mainly determined by the relative roughness of the seabed. Based on previous engineering experience, the value of the bottom friction coefficient was 0.004 to 0.008 in the calculation because the seafloor of the engineering sea area is mainly made up of fine sands. Since the water depth and topography of the proposed project area are complex, and the slope in the local area is relatively high, the wave breaking coefficient was 0.78 according to relevant specifications.

4.2. Boussinesq Equation

The Boussinesq mathematical wave model, which takes the effects of wave refraction, reflection, diffraction, and bottom friction loss caused by topography and hydraulic structures into consideration, was adopted to calculate wave conditions near the proposed breakwater and pier. The model is based on the improved numerical solution of the Boussinesq equation proposed by Madsen and Sørensen in 1992, including two modes: 2DH BW wave module (two-dimensional horizontal space coordinate) and 1DH BW wave module (one-dimensional horizontal space coordinate). The 2DH BW mode is generally used to calculate the distribution of waves in ports and coastal areas and the 1DH BW mode is usually used to calculate the wave propagation from offshore areas to beach area sso as to study the wave conditions on a certain section. The 2DH BW wave module was selected in this calculation.

4.2.1. Mathematical Equation

Based on the momentum-conservation equation and mass-conservation equation, Peregrine deduced the two-dimensional classical Boussinesq equations:

$$\frac{\partial \eta}{\partial t} + \nabla \cdot ((h+\eta)u) = 0, \tag{7}$$

$$\frac{\partial u}{\partial t} + (u \cdot \nabla)u + g\nabla\eta = \frac{1}{2}h\frac{\partial}{\partial t}\nabla(\nabla \cdot (hu)) - \frac{1}{6}h^2\frac{\partial}{\partial t}\nabla(\nabla \cdot u), \tag{8}$$

where η is the wave surface elevation; u is the average velocity of the section integrated along the water depth, namely the velocity vector of the water particle; h is the water depth; g is the acceleration of gravity; t is time.

Ge et al. [36] derived the expanded Boussinesq equation by considering the source wave-generating method, bottom friction, wave breaking, moving boundary slit method, and sponge layer technique. The modified equations are as follows:

$$\eta_t = E(\eta, u, v) + \gamma E_2(\eta, u, v) + f_s(x, y, t), \tag{9}$$

$$U_t = F(\eta, u, v) + (F_1(v))_t + \gamma(F_2(\eta, u, v)) + F^t(\eta, u_t, v_t) + F_b + F_{br} + F_{bs} + F_{sp}, \tag{10}$$

$$V_t = G(\eta, u, v) + (G_1(u))_t + \gamma(G_2(\eta, u, v)) + G^t(\eta, u_t, v_t) + G_b + G_{br} + G_{bs} + G_{sp}, \tag{11}$$

where η is the water level; h is still water depth; u and v are the horizontal velocity in x and y directions, respectively; F_b and G_b are bottom friction terms; F_{br} and G_{br} are energy dissipation terms caused by wave breaking; F_{bs} and G_{bs} are turbulent mixing considering sub-grids; F_{sp} and G_{sp} are the sponge layers used to absorb waves; γ is the linear coefficient. When $\gamma = 1$, the modified Boussinesq equation is fully nonlinear; when $\gamma = 0$, it is weak nonlinear.

4.2.2. Selection of Model Parameters

The Boussinesq mathematical equation uses the internal wave generation method, namely, the completely closed boundary is adopted to absorb the waves outside the model area by the sponge layers, which are set behind the wave growth line at the incident boundary. Based on the calculation results of the energy-balance equation wave model on a large scale, a statistical method was used to extract wave parameters from the boundary of the small scale as wave-incident conditions.

MIKE21 BW can simulate the partial reflection, absorption, and transmission of wave energy caused by structures by setting up porous layers. Due to various forms of offshore installations, reflectance characteristics are diverse. The reflectivity of a vertical breakwater is close to 100%, and that of a sloping breakwater is generally between 40% and 60%. Different reflectance characteristics are obtained by setting up the number of porous layers. The reflection coefficient of the proposed marine structure was given by the types of the breakwater and pier in this study.

The width of the sponge layer is generally 1–2 times the wave length. The absorption coefficient is given as follows:

$$C_{sponge} = \alpha^{(r^{i-1})}, i = 1, N_{sponge}, \tag{12}$$

where α and r are constants; N_{sponge} is the number of sponge layers. For the sponge layers with the thickness of 20 grids, α is usually equal to 7 and r is equal to 0.7. Sponge layers with the thickness of 20 grids were set up to absorb waves behind the wave growth line and before the land boundary and the closed boundary in this research.

5. Establishment and Verification of the Mathematical Model on a Large Scale

To ensure the availability of validation data obtained from the measured weather data and wave data, large-scale and small-scale simulations were combined for modeling, respectively. *MIKE21 SW (Spectral Waves FM)*, which is based on the energy balance equation, was adopted to simulate wave propagation of the northern Zhejiang sea area on a large scale, and *MIKE21 BW (Boussinesq Waves)*, which is based on the Boussinesq equation, was used to compute wave parameters of the construction sea area on a small scale.

5.1. Grid Division and Parameter Setting

The SW wave model was used to study the wave-height distribution on a large-scale, and the calculation area is shown in Figure 4. The model had four open boundaries: the north boundary was the South Yellow Sea, which is in the south part of Changjiang Estuary, the south boundary was Liuheng Island, the east boundary was the East China Sea, which is about 40 km away from Shengshan Island, and the west boundary wasvthe Hangzhou Bay. The solid boundary was made up of natural shoreline and measured shoreline provided by Computer Aided Design (CAD) before the implementation of the project. The Surface Water Modeling System (SMS) model was used to divide the computing area into unstructured three-point triangular grids (Figure 5), and local encryption was carried out in the engineering sea area to ensure the accuracy of the calculations.

Directionally decoupled parametric formulation was selected as the basic equation in the Spectral Waves model. In the diffraction part, the smoothing factor and number of smoothing steps were set to 1; the value of the bottom friction was considered to be constant at 0.01 according to the natural topography. In addition, the model inputs of wind and waves can be seen in Tables 1 and 3, respectively.

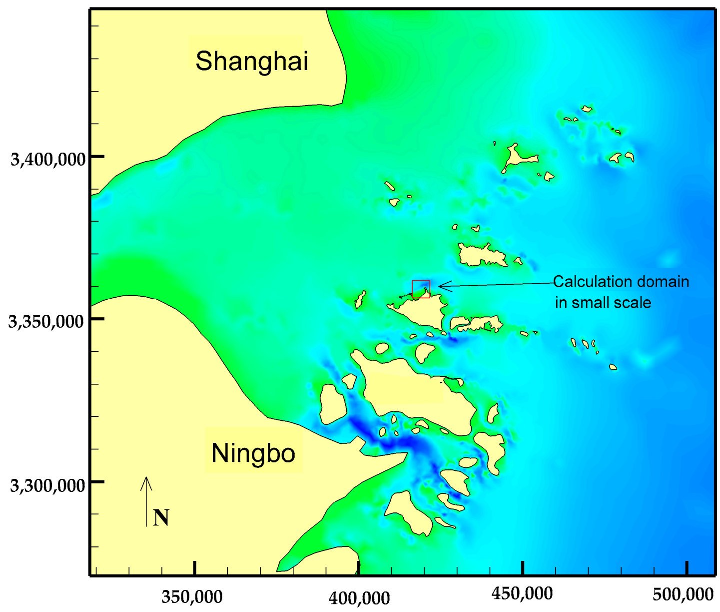

Figure 4. Calculation domain of the surface water (SW) model.

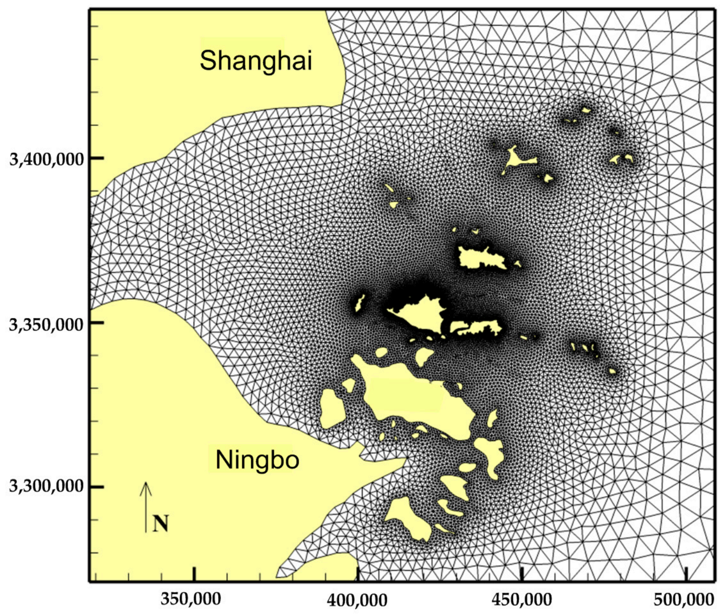

Figure 5. Grid division of SW model.

5.2. Model Verification

In the wave calculation of offshore engineering, it can be divided into 16 directions according to the wave direction. In this study, due to the blocking effect of Daishan Island in Zhoushan, the waves in five directions, SE, SSE, S, SSW, and SW, have little influence on the engineering area, so the calculation was ignored. The 11 incoming waves used on the large-scale wave mathematical model were classified according to the incident direction of waves, which were divided into waves generated by sea breeze (N, NNE, NE, ENE, E, and ESE) and waves generated by land breeze (WNW, NW, NNW, W, and WSW). Taking the design's high water level as an example, the measured values of the Shengshan ocean station and Jinjimen weather station were compared with the calculated values of the model (Figures 6 and 7).

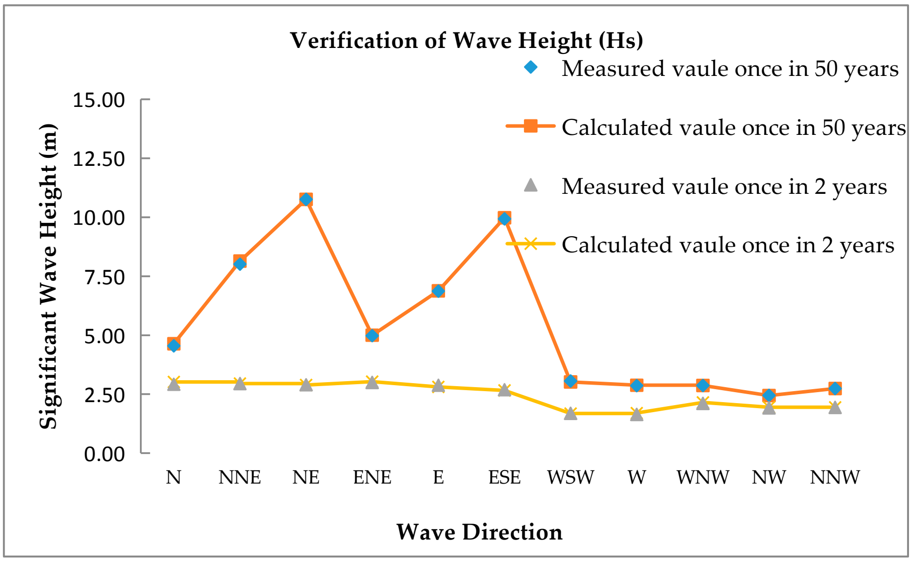

Figure 6. Verification chart of significant wave height (Hs).

It can be seen from the verification chart that the measured values and calculated values of significant wave height generated by sea breeze and land breeze have a high coincidence, respectively, however, the calculated value of significant wave period is slightly larger than the measured value but the deviation is basically within 0%–7%. Therefore, the establishment of the Spectral Waves FM wave model can better reflect wave conditions under different wave return periods and water levels in the northern Zhejiang sea area. It can provide a more accurate wave spectrum boundary condition for the Boussinesq wave model. Hence, the joint application of SW and BW models was realized.

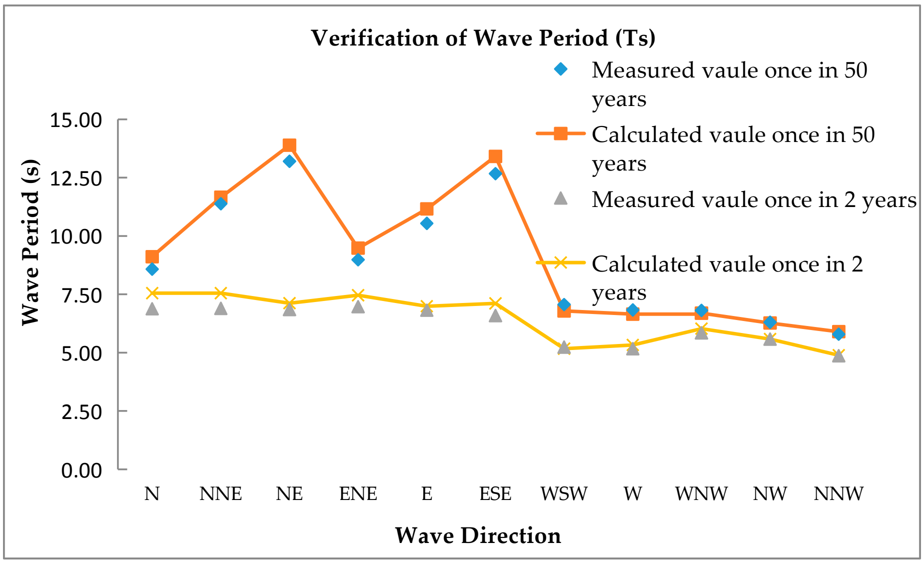

Figure 7. Verification chart of significant period (Ts).

5.3. Calculation Results on a Large Scale

The waves generated by sea breeze are large, and dissipate and attenuate continuously after entering the calculated region from the incident boundary. The wave height shows a trend of constant decrease from the deep water area to the shallow water area, which is different from the direction of the incoming wind. However, the depth of the offshore area is deeper than that near the shore, which leads to low bottom friction and a relatively low wave attenuation. When a wave generated by land breeze enters the computational domain, distribution of wave height increases from the shallow water area to the deep water area on the whole, which is the same as the incoming wind. Six wave directions, N, NNE, NE, W, WNW, and NW, that have great influence on the project were selected for calculation. The distribution characteristics of the wave field are shown in Figure 8.

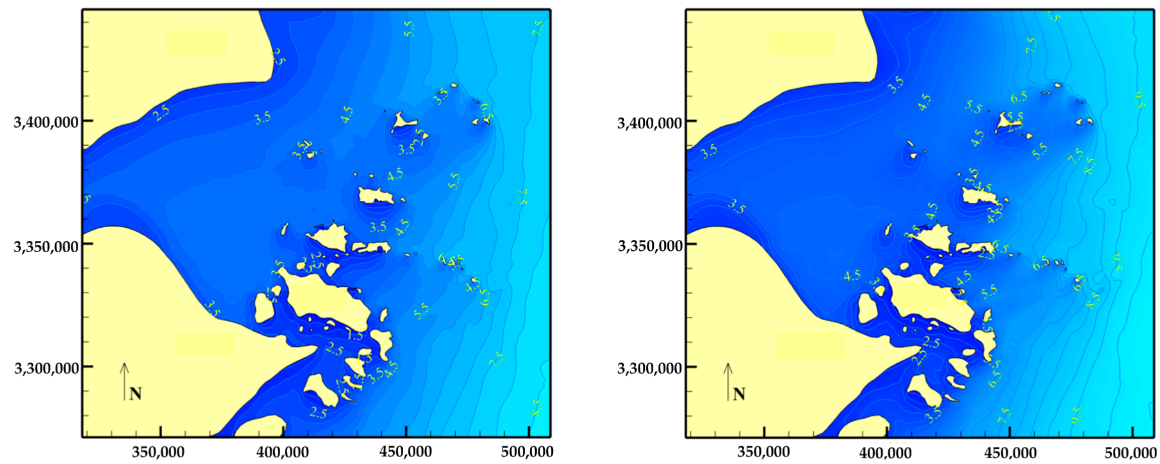

(**a**) N (**b**) NNE

Figure 8. *Cont.*

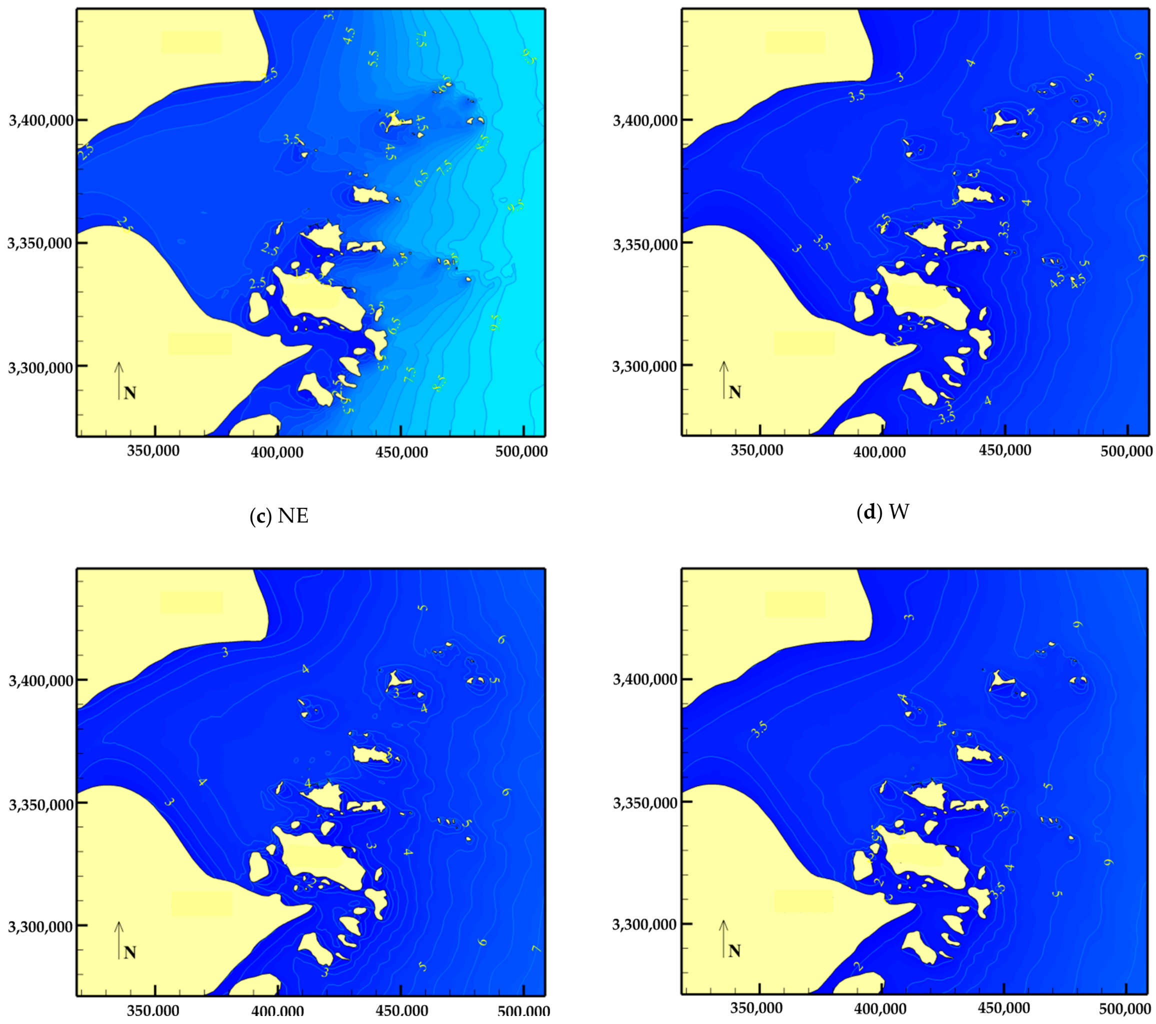

(**c**) NE (**d**) W

(**e**) WNW (**f**) NW

Figure 8. Distribution of significant wave height on a large scale before engineering.

Figure 8a–f shows the change of wave height contours of different incident wave directions when the waves propagate from the outer sea to the offshore area. It can be clearly seen from the figures that the wave height values of N, NNE, and NE in the outer sea are significantly higher than those of the other three directions. The reasonable distribution of wave field on a large-scale is a prerequisite to ensure the accuracy of simulation results on a small-scale.

6. Establishment and Application of the Mathematical Model on a Small Scale

During the propagation of waves from deep water to offshore areas, wave characteristics are constantly changing due to the influence of wave deformations, such as refraction, diffraction, reflection, energy dissipation, and breaking. In order to fully consider the above processes and their influence on the proposed project, an appropriate wave mathematical model is necessary to calculate the wave distribution in the target area. In this study, the *MIKE21 Boussinesq Waves* mode based on the Boussinesq equation was applied to predict wave changes on a small scale before and after the implementation.

6.1. Grid Division and Parameter Setting

On the basis of accurate calculation results on a large scale, open boundary direction and computational domain size were adjusted according to different directions of incident waves to adapt to the requirements of calculation (Figure 9). The BW model divides the computing area into rectangular meshes. In this study, each grid was a square with sides of 6 m in length, and there were 12 grid nodes within one wavelength to satisfy the computational conditions of the Boussinesq equation. Sponge layers with a thickness of 20 grids were set around the non-solid boundary in the engineering area for wave absorption. Porous layers with thickness of 3 grids were set at the junction of the shoreline and water, and porosity was estimated by the *MIKE21* Toolbox. In addition, internal wave generation was set at the open boundary as the initial value of the model input. Based on the topographic and bathymetric data of the engineering area, the Setup Planner tool was used to obtain the minimum wave period of 9.7 s and time step of 0.225 s in the calculation domain.

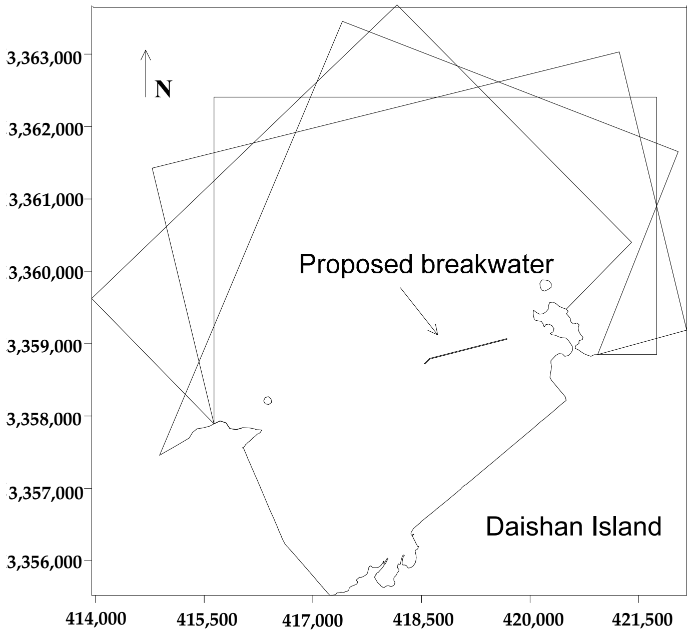

Figure 9. Schematic diagram of different wave directions in the computational domain.

6.2. Engineering Application

The proposed pier and breakwater are located in the north of Daishan Island. Two plane-layout schemes were designed with a fixed position of the pier but different lengths and azimuths of the breakwater. Then, the influence of the breakwater on the wave field under different conditions were discussed in order to provide reasonable simulation results for the unit in charge of construction (Table 4). The layout of the breakwater with different azimuths and lengths is shown in Figure 10.

Table 4. Layout of the breakwater.

Calculation Scheme	Layout of Breakwater
Scheme 1	The total length of the breakwater is 1200 m: the broken line section on the west side is 100 m long, and that on the east is 1100 m long.
Scheme 2	The total length of the breakwater is 1300 m: the broken line section on the west side is 100 m long, and that on the east is 1200 m long. In addition, Scheme 2 was rotated 8 degrees counterclockwise along the axis on the basis of Scheme 1.

6.2.1. Distribution of the Wave Field

The waves in the N, NNE, NE, W, WNW, and NW directions that emerge once in 50 years under the condition of an extreme high water level and the distribution of significant wave height before the implementation of the project and after the implementation of Scheme 1 and Scheme 2 are shown in Figures 11–16. It should be noted that the wave height diagrams only reflect the wave conditions within the range of about 10 km around the proposed project, and the unit is meters.

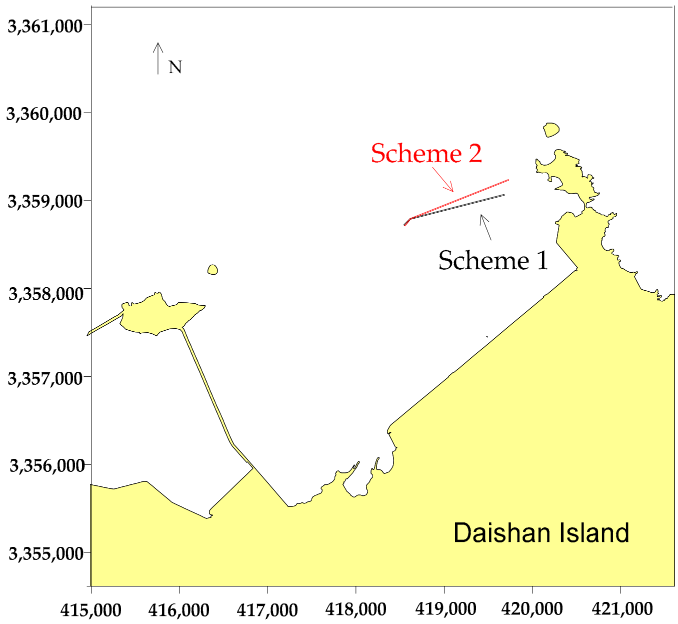

Figure 10. Layout of the breakwater.

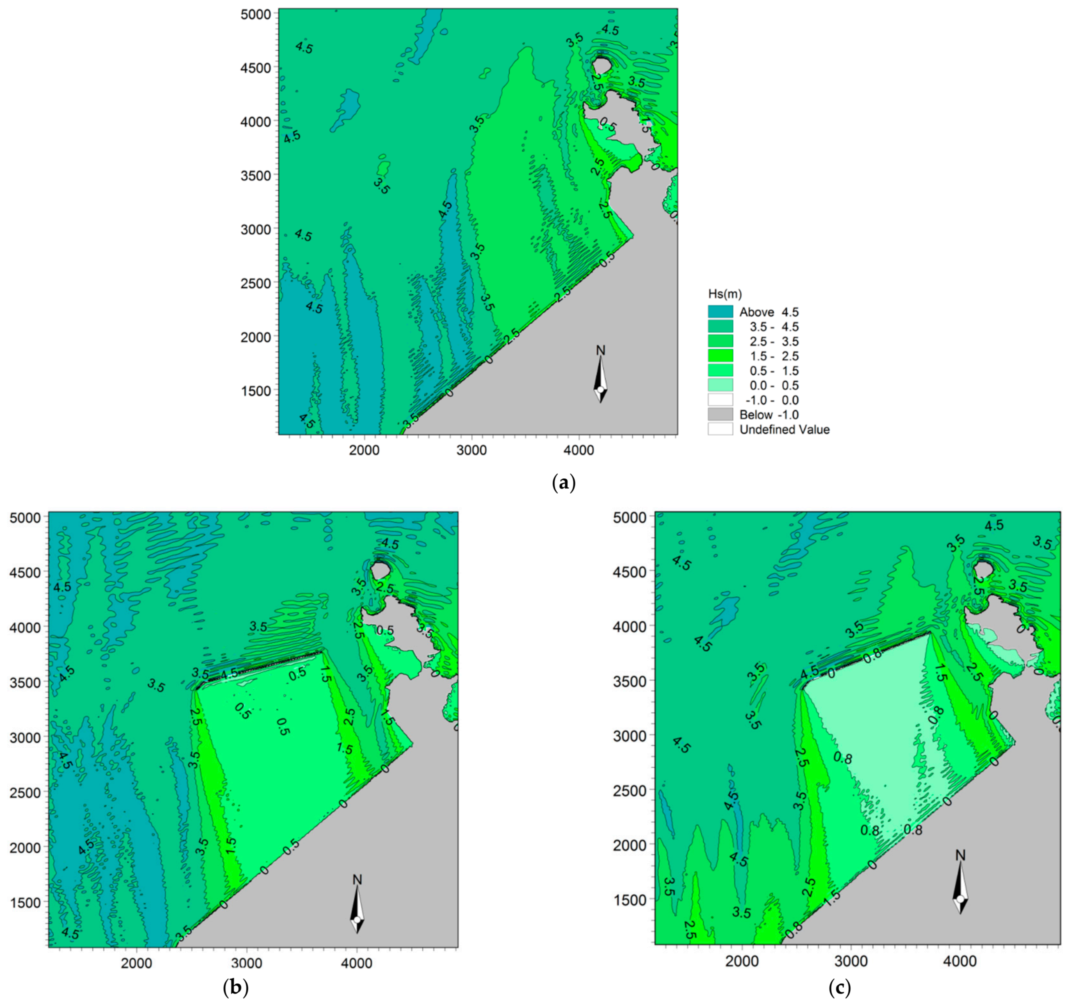

Figure 11. Distribution of significant wave height in the N direction under three working conditions: (**a**) before the project, (**b**) Scheme 1, (**c**) Scheme 2. Notes: In the figure, wave height vaules and plane coordinates are all in meters.

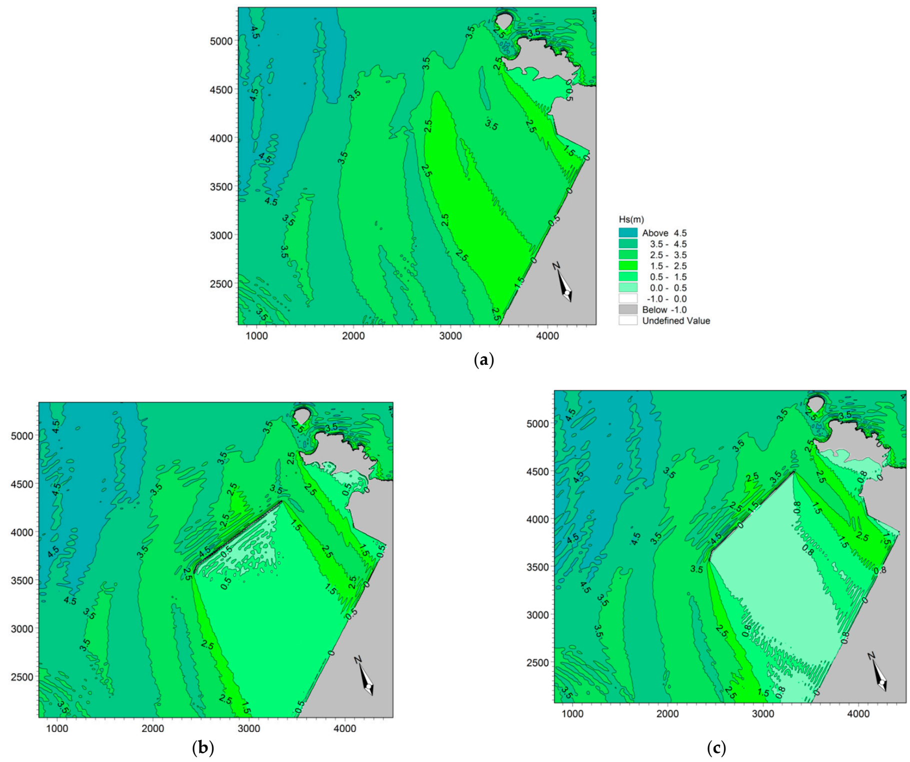

Figure 12. Distribution of significant wave height in the NNE direction under three working conditions: (**a**) before the project, (**b**) Scheme 1, (**c**) Scheme 2. Notes: In the figure, wave height vaules and plane coordinates are all in meters.

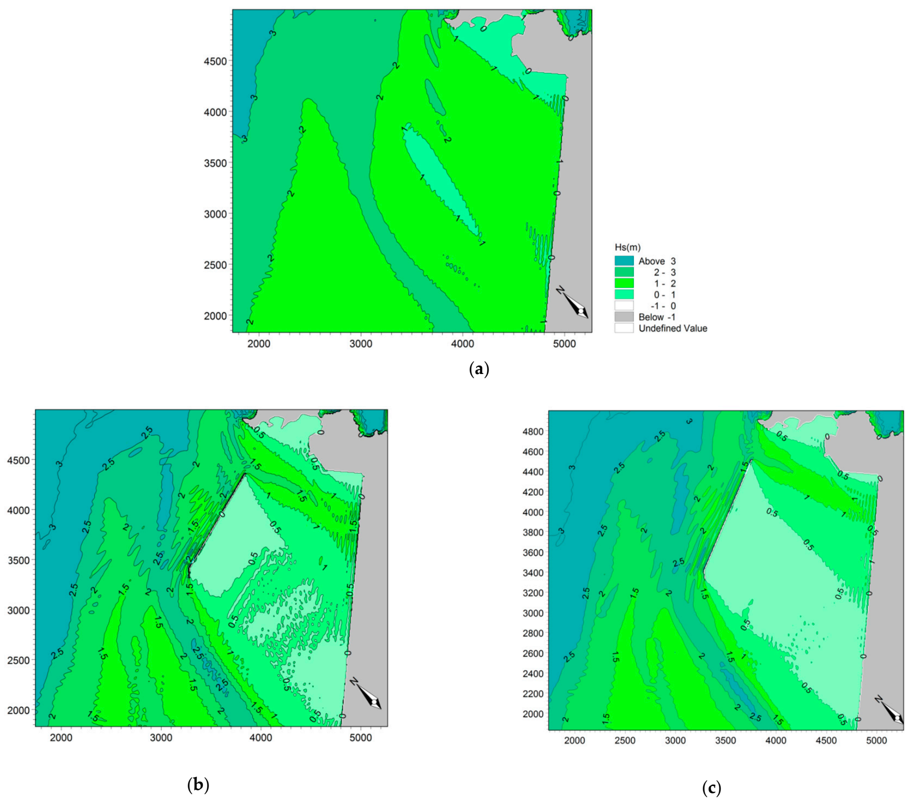

Figure 13. Distribution of significant wave height in the NE direction under three working conditions: (**a**) before the project, (**b**) Scheme 1, (**c**) Scheme 2. Notes: In the figure, wave height vaules and plane coordinates are all in meters.

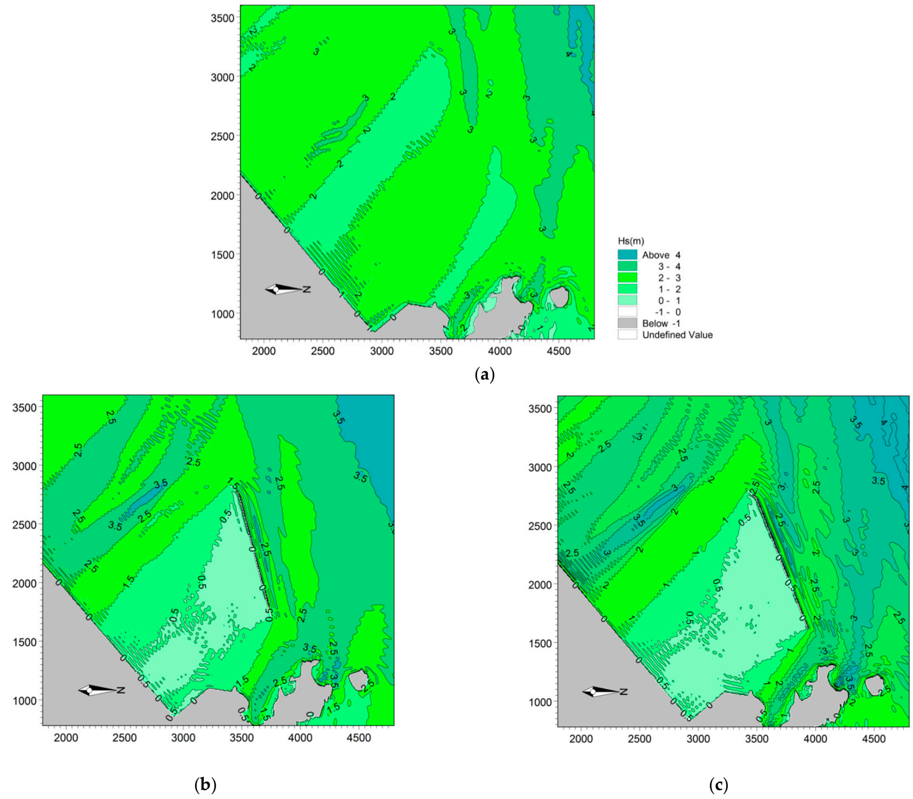

Figure 14. Distribution of significant wave height in the W direction under three working conditions: (**a**) before the project, (**b**) Scheme 1, (**c**) Scheme 2. Notes: In the figure, wave height vaules and plane coordinates are all in meters.

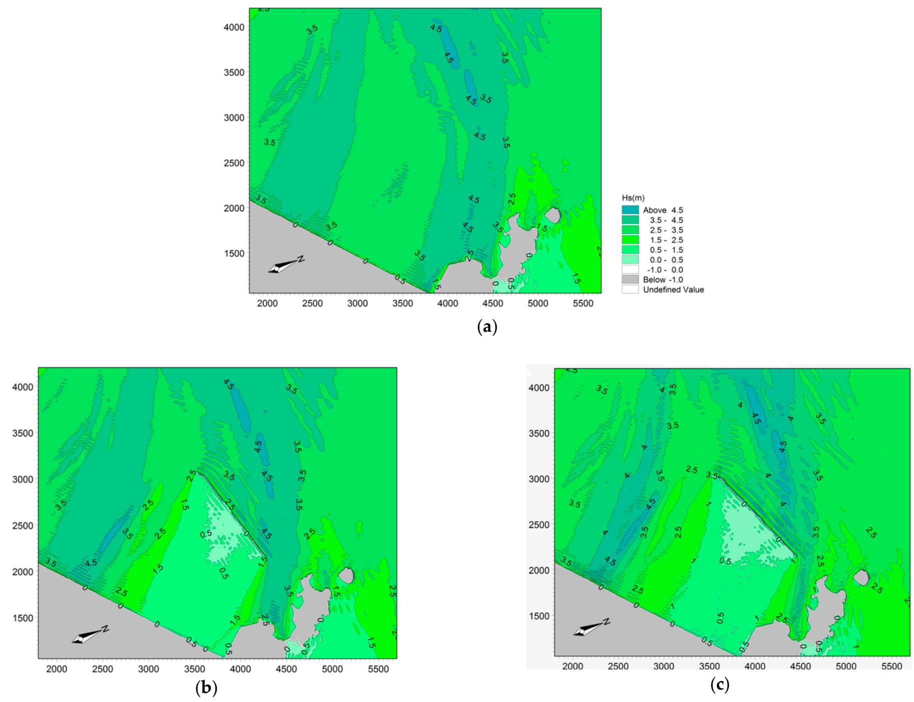

Figure 15. Distribution of significant wave height in the WNW direction under three working conditions: (**a**) before the project, (**b**) Scheme 1, (**c**) Scheme 2. Notes: In the figure, wave height vaules and plane coordinates are all in meters.

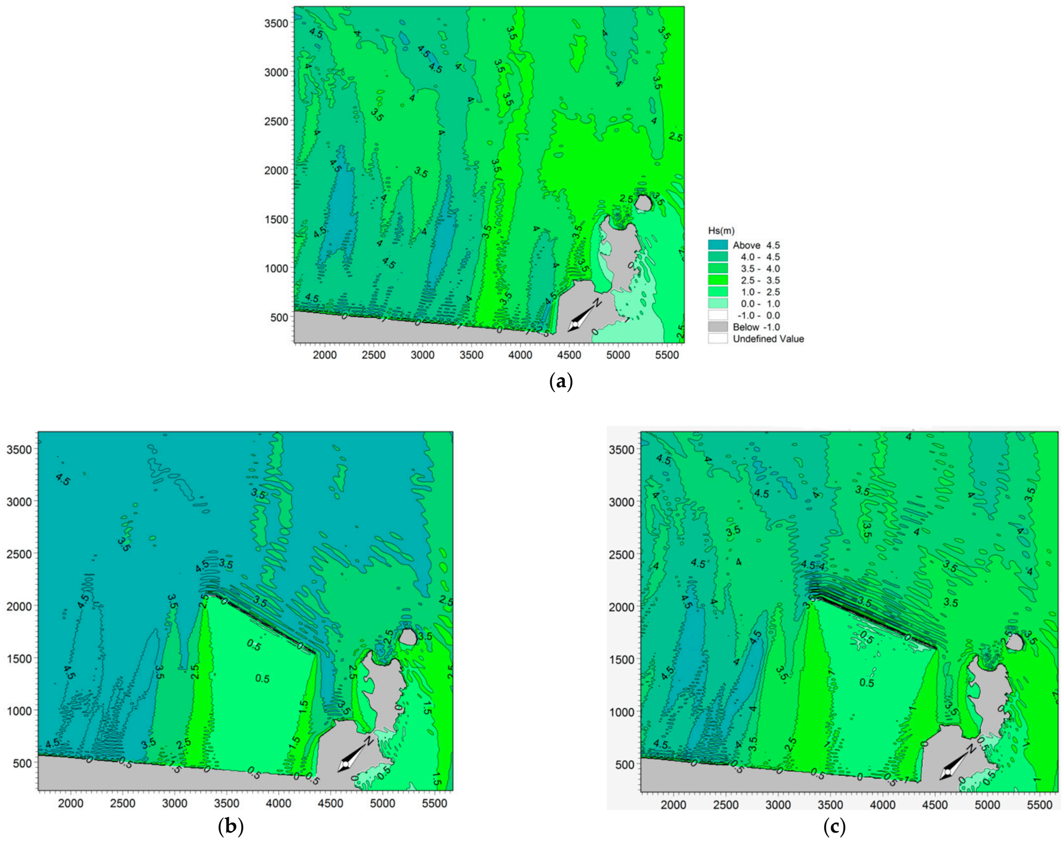

Figure 16. Distribution of significant wave height in the NW direction under three working conditions: (**a**) before the project, (**b**) Scheme 1, (**c**) Scheme 2. Notes: In the figure, wave height vaules and plane coordinates are all in meters.

It can be seen from Figures 11–16 that the distribution of significant wave height of the six wave directions under three working conditions are different. Before the project, wave height was relatively large through the whole calculation domain; after the implementation of Scheme 1, wave height near the breakwater would be lower to some extent; with the implementation of Scheme 2, the wave height would lower, and a better cover water area would be formed. Thus, the optimization of the breakwater can provide sufficient security for passenger transport.

6.2.2. Wave Parameters of Feature Points

In order to obtain wave parameters under different combination calculations, 14 wave feature points were arranged at about 20 m in front of the proposed breakwater and about 30 m behind the breakwater on the basis of Scheme 1 and were named O_1–O_{14}, successively (Figure 17); in addition, five feature points were arranged about 30 m in front of the proposed pier front and named W_1–W_5, successively (Figure 18). Plane coordinates of the wave feature points are given in Table 5.

The topographic conditions of the construction sea area are relatively complex. The north, northeast, northwest, and west sides of Yanwo Island are open water areas without shelter of any islands. However, the east, southeast, south, and southwest sides have better shielding conditions due to the shelter of Daishan Island. For overall analysis of wave parameters near the proposed breakwater under different layouts and engineering conditions, the variation trends of significant wave height above 14 wave feature points were compared and analyzed (Figure 19).

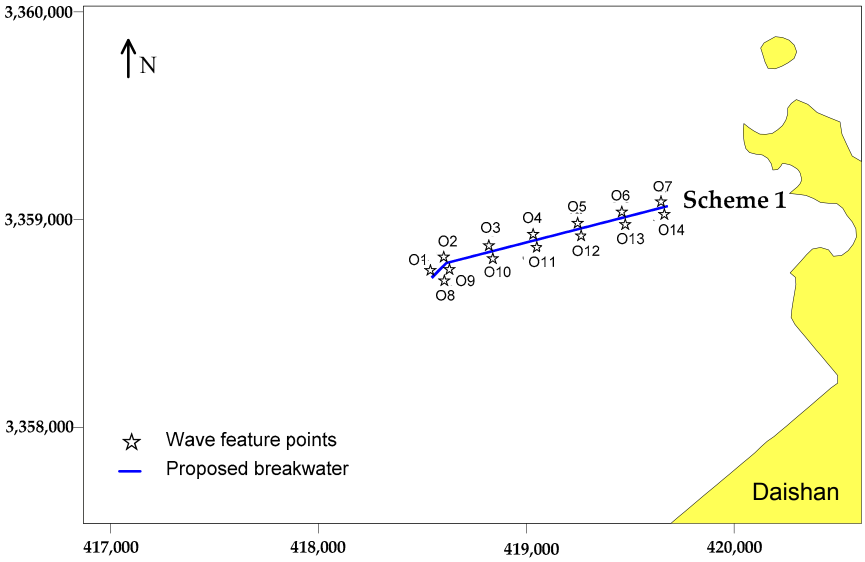

Figure 17. Wave feature points of the breakwater.

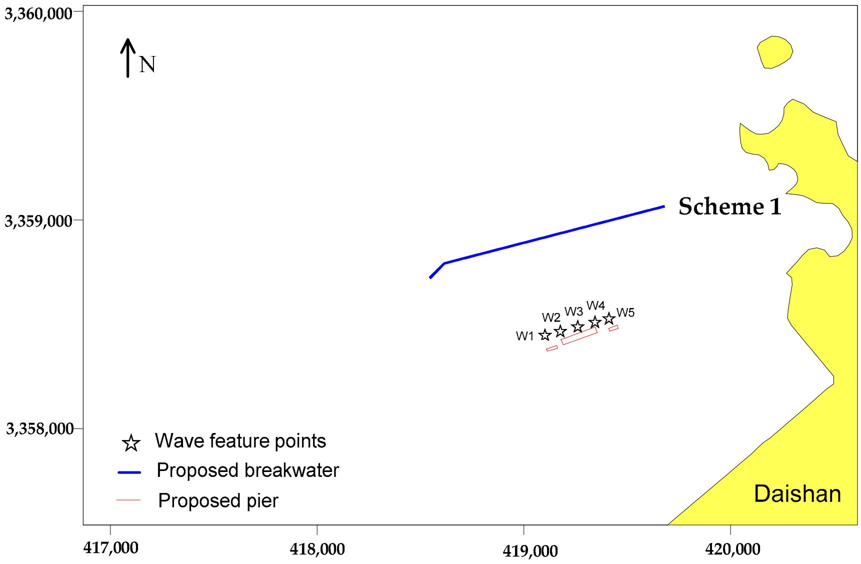

Figure 18. Wave feature points of the pier.

Table 5. Plane coordinates of the wave feature points (unit: m).

Location of Feature Points	Feature Points	*x*-Coordinate	*y*-Coordinate	Feature Points	*x*-Coordinate	*y*-Coordinate
Both sides of the breakwater	O_1	418,535.9	3,358,763.6	O_8	418,603.9	3,358,714.0
	O_2	418,601.6	3,358,828.1	O_9	418,625.8	3,358,768.2
	O_3	418,819.5	3,358,883.5	O_{10}	418,836.8	3,358,818.9
	O_4	419,031.6	3,358,938.8	O_{11}	419,048.9	3,358,875.4
	O_5	419,244.9	3,358,990.7	O_{12}	419,261.0	3,358,930.7
	O_6	419,458.2	3,359,044.9	O_{13}	419,474.3	3,358,984.9
	O_7	419,647.2	3,359,093.3	O_{14}	419,661.1	3,359,033.3
Pier front	W_1	419,103.9	3,358,447.1	W_4	419,343.5	3,358,511.0
	W_2	419,178.0	3,358,468.9	W_5	419,411.7	3,358,528.4
	W_3	419,262.2	3,358,490.7			

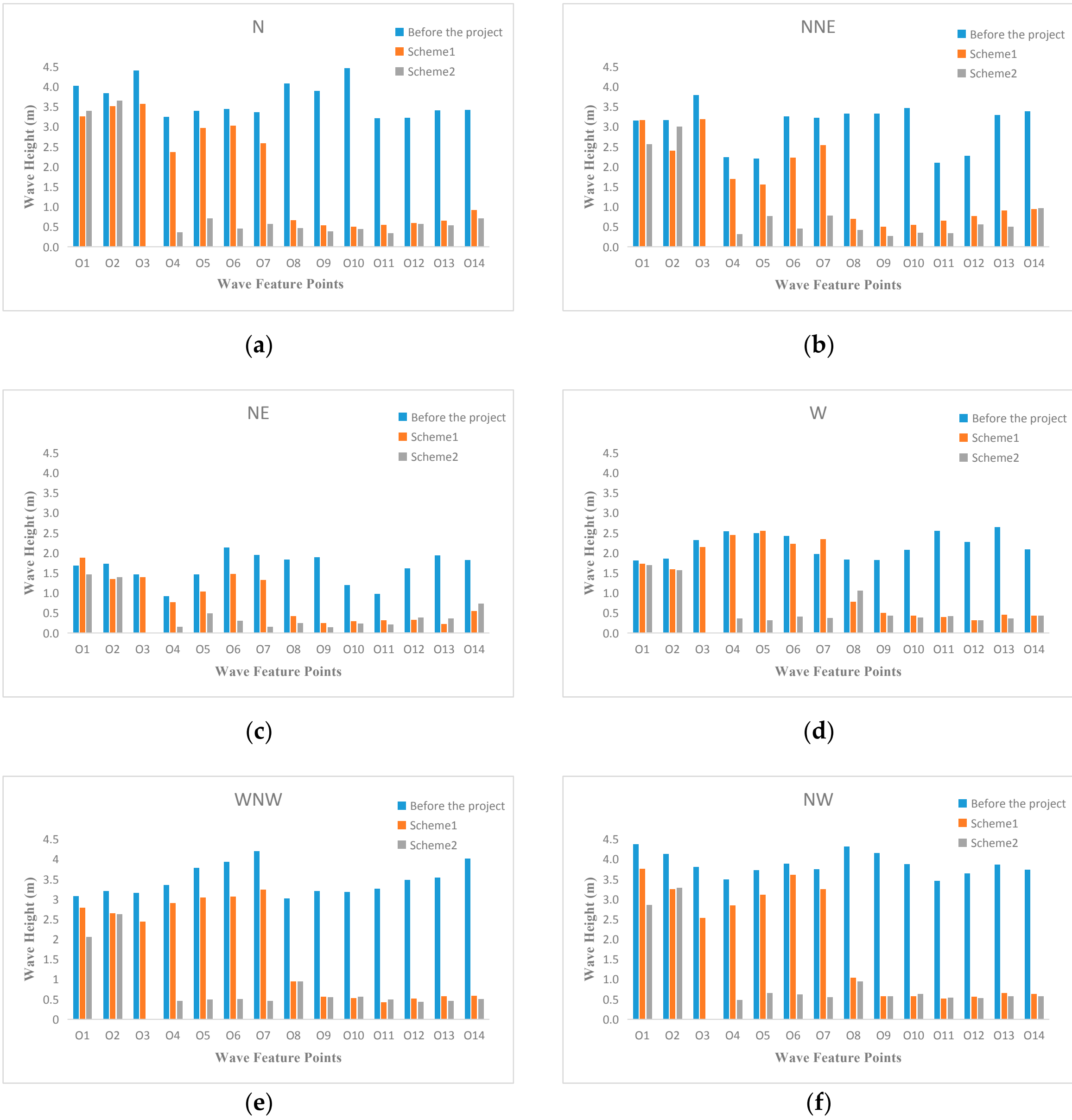

Figure 19. Wave parameters at the feature points of different schemes. (**a**) wave height vaules of wave coming from N direction at O_1–O_{14} under three working conditions, (**b**) wave height vaules of wave coming from NNE direction, (**c**) wave height vaules of wave coming from NE direction, (**d**) wave height vaules of wave coming from W direction, (**e**) wave height vaules of wave coming from WNW direction, (**f**) wave height vaules of wave coming from NW direction.

It can be seen from the histograms that before the implementation of engineering, wave height is relatively high when the incident wave direction is N (Figure 19a), NNE (Figure 19b), WNW (Figure 19e), and NW (Figure 19f). The significant wave heights are all above 3.7 m, and the maximum wave height appears at feature points O_{10}, O_3, O_7, and O_1 with the corresponding values of 4.46 m, 3.79 m, 4.20 m, and 4.37 m, respectively. Since there are Dongken Island and umbrella reef on the west side, Yanwo mountain and its affiliated reefs on the east side, Daishan Island on the south side, and unshielded sea area on the north and northwest sides in the engineering sea area, the above-mentioned waves can be propagated forward to the proposed breakwater and pier. In addition, the deeper water depth, slow bottom slope, low wave energy dissipation in the northwest, and reflection effect of Daishan Island lead to larger waves of more than four incident directions. Because of the shielding effect of Yanwo Island, the energy dissipation of waves generated from the NE is large when it propagates from the outer sea towards the engineering sea area, and the maximum wave height at the front of the breakwater is only 2.14 m (Figure 19c). Refraction and diffraction occur due to the obstruction of Dongken Island when the waves generated from W propagate from shallow water to deep water, and the wave attenuation is smaller than that in the NE direction, and the maximum wave height is 2.64 m at the front of the breakwater (Figure 19d).

Height value at the wave feature points will be greatly reduced after the implementation of the project compared with that before the project in Figure 19, indicating that the breakwater can effectively block waves. Comparing the two construction schemes, it was found that the performance of Scheme 2 in protecting the water area behind the breakwater is better than Scheme 1. In particular, the feature point O_3 is on the axis on the rotating breakwater, so there are no wave height values in the histograms (Figure 19a–f).

6.2.3. Covering Area of the Breakwater

In order to demonstrate the importance of changing the length and axis of the breakwater, the covering area of the breakwater was statistically analyzed under the two schemes to optimize the plane layout. Sea area with wave height less than 0.6 m behind the breakwater and its corresponding change rate are shown in Table 6.

Table 6. Area table.

Schemes	Statistical Indexes	N	NNE	NE	W	WNW	NW
Scheme 1	Covering area (km^2)	0.37	0.52	1.31	1.03	0.43	0.19
Scheme 2	Covering area (km^2)	0.69	0.80	2.06	1.32	0.88	0.30
	Rate of change (%)	88.51	53.90	56.78	28.30	103.36	55.97

The statistical results show that compared with Scheme 1, Scheme 2, which is extended 100 m along the long straight embankment to the east and is rotated 8 degrees counterclockwise along the axis on the basis of Scheme 1, can improve the sheltered area of incident waves in the N, NNE, NE, W, WNW, and NW directions, and the coverage area with wave height less than 0.6 m on the back of the breakwater can be increased by 88.51%, 53.9%, 56.78%, 28.3%, 103.36%, and 55.97%, respectively. In view of the above analysis, the anti-clockwise rotation and eastward extension of the breakwater have a significant impact on wave height behind the breakwater, and the longer the extension section, the better the improvement effect. In Scheme 2, the coverage area is increased by about a quarter in the W direction, which is the weakest direction of improvement; however, the sheltered area is nearly doubled in the WNW direction compared with Scheme 1.

6.2.4. Ship Berthing Stability Analysis

The influence of incident waves in different directions on the wave field of the proposed project was quite different, so the berthing stability of the pier front in different wave directions was assessed under the condition of design high water level. In accordance with the rules on allowable wave height and wind power of ship operation in the Harbour Master Design Specifications (JTS165-2013) [37], the simulation results of each incident wave were converted into $H_{1/10}$ wave height for berthing stability analysis according to the conversion relationship among various accumulated frequency wave heights in the Hydrological Specifications for Ports and Waterways (JTS145-2015) [38]. The regulations recommend that the allowable wave heights for both loading and unloading operations of ships should be less than 0.6 m. W_1 to W_5 represent the berthing status of ships (Tables 7 and 8), where "Y" stands for safe berthing of ships and "N" means unsafe berthing.

Table 7. Berthing stability analysis of Scheme 1 (unit: m). Y stands for safe berthing of ships and N means unsafe berthing.

	W_1		W_2		W_3		W_4		W_5	
N	0.5	Y	0.56	Y	0.57	Y	0.51	Y	0.5	Y
NNE	0.45	Y	0.44	Y	0.46	Y	0.43	Y	0.45	Y
NE	0.34	Y	0.32	Y	0.29	Y	0.29	Y	0.27	Y
W	0.52	Y	0.45	Y	0.34	Y	0.29	Y	0.26	Y
WNW	0.84	N	0.66	N	0.51	Y	0.52	Y	0.43	Y
NW	0.89	N	0.76	N	0.59	Y	0.58	Y	0.56	Y

Table 8. Berthing stability analysis of Scheme 2 (unit: m). Y stands for safe berthing of ships and N means unsafe berthing.

	W_1		W_2		W_3		W_4		W_5	
N	0.34	Y	0.33	Y	0.32	Y	0.35	Y	0.41	Y
NNE	0.27	Y	0.28	Y	0.35	Y	0.37	Y	0.39	Y
NE	0.24	Y	0.25	Y	0.28	Y	0.25	Y	0.24	Y
W	0.58	Y	0.53	Y	0.39	Y	0.33	Y	0.28	Y
WNW	0.59	Y	0.56	Y	0.5	Y	0.46	Y	0.43	Y
NW	0.58	Y	0.57	Y	0.53	Y	0.55	Y	0.51	Y

According to the statistical analysis of wave parameters at the proposed pier, it can be concluded that only WNW and NW incident waves do not meet the requirement of $H_{1/10}$ wave height less than 0.6 m at W_1 and W_2 points.

After the implementation of Scheme 2, wave heights of each directional incident waves at the pier front can meet the requirement that $H_{1/10}$ wave height is less than 0.6 m, and ships can safely load and unload. Compared with Scheme 1, it not only reduces the height value of the feature points, but also improves the disadvantage that WNW and NW incident waves cannot berth stably at W_1 and W_2 points.

7. Discussion and Conclusions

According to two layouts of the proposed breakwater, combined with the large-scale and small-scale wave models that we established, results and analysis have led to the following conclusions.

Based on the wave field distribution and the variation of wave parameters at the feature points, it can be seen that wave height behind the breakwater would be significantly lower than it was before the project if the proposed project is implemented, and Scheme 2 would have a better improvement effect on wave conditions (Figures 11–16 and Figure 19); Scheme 2 would have a significant improvement in shielding effect of the waters behind the breakwater, especially for the N and WNW incident waves with the coverage area nearly doubled compared with Scheme 1 (Table 6); after the implementation of Scheme 1, W_1 and W_2 points would exceed the allowable operational wave height (Table 7),while each feature point could safely berth after the implementation of Scheme 2 (Table 8). The hydrodynamic environment changes of Schemes 1 and 2 in the engineering sea area were compared by considering the distribution of wave field, changes of wave parameters at feature points, coverage area, and ship berthing stability, and it can be concluded that the shielding effect to sea waves of Scheme 2 is better than that of Scheme 1. Scheme 2 is a more reasonable plane layout.

In summary, the layouts of the breakwater have little influence on wave the field on a large-scale, but the impact is mainly concentrated near the engineering area. In this paper, four aspects were considered so as to reliably select the optimal scheme of the proposed breakwater.

In future studies, the influence of sediment movement should be studied in order to discuss the effects of different parameters to numerical simulation results. Moreover, a series of computational schemes will be added in order to make the project planning more reasonable.

Author Contributions: H.G. finished the first draft of the paper and completed the calculation and verification of mathematical models; F.L. and R.L. edited and reviewed the manuscript and provided language editing services; X.D. supervised the setting of model parameters; Y.Z. dealt with the raw data.

Funding: This work was supported by the National Natural Science Foundation of China (Grant No.41276017), the Marine Science and Technology Innovation Program of Jiangsu (Grant NO.HY2018-1 and HY2017-2), the Postgraduate Research & Practice Innovation Program of Jiangsu Province (Grant No.KYCX18-0522), and the Fundamental Research Funds for the Central Universities (Hohai University) (Grant No.2018B703X14).

Conflicts of Interest: The authors declare no conflict of interest.

References

1. Gu, H.; Sun, J.; Zheng, B.; Chen, H. Developments of Near-shore Wave Numerical Models. *J. Waterw. Harb.* **2004**, *25*, 78–83.
2. Huang, H. A Review of Coastal Wave Modelling. *Adv. Mech.* **2001**, *31*, 592–610.
3. Jiang, S. Analysis of Wave Radiation Stress Theory and Its Applicability. Ph.D. Thesis, Hohai University, Nanjing, China, June 2011.
4. Ye, Y. The Numerical Simulation of Wind Waves in Taiwan Strait. Master's Thesis, Xiamen University, Xiamen, China, June 2006.
5. Feng, M.; Sha, W.; Zhu, S. Study on Some Numerical Methods Calculating Waves in Shore. *Mar. Forecast.* **2003**, *20*, 52–59.
6. Berkhoff, J.C. Computation of combined refraction-diffraction. In Proceedings of the 13th International Conference on Coastal Engineering, Vancouver, BC, Canada, 10–14 July 1972; pp. 796–814.
7. Miles, J.W. On the generation of surface waves by shear flows. *J. Fluid Mech.* **1957**, *3*, 163–175. [CrossRef]
8. Hasselmann, K. On the spectral dissipation of ocean waves due to white capping. *Bound.-Layer Meteorol.* **1974**, *6*, 107–127. [CrossRef]
9. Liang, L. Numerical Simulations of Typhoon Waves in the Sea Area around Zhoushan. Master's Thesis, Hohai University, Nanjing, China, June 2015.
10. Liu, P.L.F. Model equations for wave propagations from deep to shallow water. *Adv. Coast. Ocean Eng.* **1995**, *1*, 125–157.
11. Zhang, W. Study on the Suspension Flux of Substance in Nearshore and Its Application in Jiangsu Sea Area. Ph.D. Thesis, Hohai University, Nanjing, China, June 2013.
12. Dalrymple, R.A.; Kirby, J.T. Models for very wide angle water waves and wave diffraction. *J. Fluid Mech.* **1988**, *192*, 33–50. [CrossRef]
13. Song, Z.; Zhong, H.; Yan, Y. *The 8th National Coastal Engineering Symposium*; Ocean Press: Beijing, China, 1997; pp. 320–327.
14. Li, R.; Wei, S.; Wang, L.; Meng, X. A Mathematical Model to Simulate Nearshore Wave Transformation. *Ocean Eng.* **1998**, *16*, 49–55.
15. Hong, G.; Feng, W.; Zhang, H. Numerical Modelling of Wave Propagation in Water of Varying Topography and Current. *J. Hohai Univ. Nat. Sci.* **1999**, *2*, 1–9.
16. Yin, B.S.; Yang, D.Z.; Sha, R.N.; Cheng, M.H. Improvement of different source function expressions in SWAN model for the Bohai Sea. *Prog. Nat. Sci.* **2005**, *15*, 720–724.
17. Hu, K.; Ding, P.; Zhu, S. Numerical simulation of typhoon waves around the waters of the Changjiang Estuary A case study of Typhoon Rusa and Typhoon Sinlaku. *Acta Oceanol. Sin.* **2004**, *26*, 23–33.
18. Xu, F.; Yan, Y.; Zhang, C. Wave numerical model for shallow water. *China Ocean Eng.* **2000**, *14*, 193–202.
19. Cuchiara, D.C.; Fernandes, E.H.; Strauch, J.C.; Winterwerp, J.C.; Calliari, L.J. Determination of the wave climate for the Southern Brazilian shelf. *Cont. Shelf Res.* **2009**, *29*, 545–555. [CrossRef]
20. Ou, S.H.; Liau, J.M.; Hsu, T.W.; Tzang, S.Y. Simulating typhoon waves by SWAN wave model in coastal waters of Taiwan. *Ocean Eng.* **2002**, *29*, 947–971. [CrossRef]
21. Tolman, H.L. Treatment of unresolved islands and ice in wind wave models. *Ocean Model.* **2003**, *5*, 219–231. [CrossRef]
22. Hemer, M.A.; Simmonds, I.; Keay, K. A classification of wave generation characteristics during large wave events on the Southern Australian margin. *Cont. Shelf Res.* **2008**, *28*, 634–652. [CrossRef]
23. Qi, Y.; Zhu, B.; Shi, P. Analysis of significant wave heights from WWATCH and TOPEX/Poseidon Altimetry. *Acta Oceanol. Sin.* **2003**, *25*, 1–9.

24. Zhou, L.; Wang, A.; Guo, P.; Wang, Z. Effect of surface waves on air–sea momentum flux in high wind conditions for typhoons in the South China Sea. *Prog. Nat. Sci.* **2008**, *18*, 1107–1113. [CrossRef]
25. Xu, F.; Perrie, W.; Toulany, B.; Smith, P.C. Wind-generated waves in Hurricane Juan. *Ocean Model.* **2007**, *16*, 188–205. [CrossRef]
26. Gao, S.; Ding, P.; Zhu, S. Operating System Transplantation of WaveWatch and Modification of Its Nesting Interface With SWAN. *Adv. Mar. Sci.* **2006**, *24*, 228–237.
27. Rogers, W.E.; Kaihatu, J.M.; Hsu, L.; Jensen, R.E.; Dykes, J.D.; Holland, K.T. Forecasting and hindcasting waves with the SWAN model in the Southern California Bight. *Coast. Eng.* **2007**, *54*, 1–15. [CrossRef]
28. Shu, X. Wind Wave and Offshore Wave Transformation Considering Nonlinear Dispersion Effect and Its Application. Ph.D. Thesis, Hohai University, Nanjing, China, June 2009.
29. Wang, S.; Li, R.; Ji, M.; Dong, X.; Zhu, W. Combined application of SWAN and CGWAVE model in calculation of design wave parameters. *J. Waterw. Harb.* **2015**, *4*, 308–312.
30. Wang, Y.; Wang, J.; Kang, Y.; Hao, J. Plane arrangement scheme of breakwater for Xiaoguoju Fishing Port project. *Port Waterw. Eng.* **2018**, *3*, 86–92.
31. Xu, J.; Fang, C.; Huang, L.; Tu, Y. Analysis of the impact of navigation upon wave propagation by using MIKE 21 BW module. *J. China Inst. Water Resour. Hydropower Res.* **2011**, *9*, 292–297.
32. Ji, Q.; Dong, S. Modelling Wave Transmission and Overtopping Based on Energy Balance Equation. *J. Ocean Univ. China* **2018**, *17*, 1033–1043. [CrossRef]
33. Zapata, C.; Puente, A.; García, A.; García-Alba, J.; Espinoza, J. The Use of Hydrodynamic Models in the Determination of the Chart Datum Shape in a Tropical Estuary. *Water* **2019**, *11*, 902. [CrossRef]
34. Liu, W.; Ning, Y.; Zhang, Y.; Zhang, J. Shock-Capturing Boussinesq Modelling of Broken Wave Characteristics Near a Vertical Seawall. *Water* **2018**, *10*, 1876. [CrossRef]
35. *Technical Regulations on Seawall Engineering of Zhejiang Province*; Zhejiang Department of Water Resources: Zhengjiang, China, 1999.
36. Ge, W.; James, T.K. Time-Dependent Numerical Code For Extended Boussinesq Equations. *J. Waterw. Port Coast. Ocean Eng.* **1995**, *121*, 251–261.
37. *Harbour Master Design Specifications (JTS165-2013)*; China Communications Press: Beijing, China, 2014.
38. *Hydrological Specifications for Ports and Waterways (JTS145-2015)*; China Communications Press: Beijing, China, 2015.